THE JOURNAL OF PHYSICAL CHEMISTRY C
A JOURNAL OF THE AMERICAN CHEMICAL SOCIETY

pubs.acs.org/JPCC
Article

Site-Dependent Oxidation States of Single Cobalt Atoms in a Porphyrin-Based Monolayer on Graphene

Davide Bidoggia, Francesco Armillotta, Alessandro Sala, Erik Vesselli, and Maria Peressi*

Cite This: J. Phys. Chem. C 2024, 128, 1737−1745
Read Online

ABSTRACT: We investigate a layer of cobalt tetrapyridyl porphyrins (CoTPyPs) self-assembled on an almost freestanding graphene (GR) sheet supported by Ir(111) with complementary experimental techniques and density functional theory (DFT) ab initio simulations. Beside the metal atoms enclosed within the porphyrin macrocycles, additional Co atoms can be accommodated at the molecular network's interstice via physical vapor deposition and can bind up to four adjacent molecules. Therefore, such a system presents two metallic sites, both tetra-coordinated to nitrogen atoms. At the same time, a rearrangement of the network occurs depending on the coverage of such additional atoms. The bare CoTPyPs arrange themselves on GR in an almost hexagonal close-packed pattern with alternating orientations. The addition of extra Co atoms causes a dramatic transformation in the network. At full peripheral metal coverage (i.e., one additional Co per CoTPyP), the network drastically changes becoming almost square. Intermediate coverages display different peculiar patterns characterized by unique chiral structures. Importantly, our DFT calculations reveal a remarkable effect on the system's work function attributed to the presence of these additional metal atoms, despite their extremely small amount even at full coverage (less than 2% of a monolayer with respect to the number of carbon atoms in the GR sheet). Furthermore, we report a different behavior of the two Co sites showing different oxidation states and molecular orbital occupations.

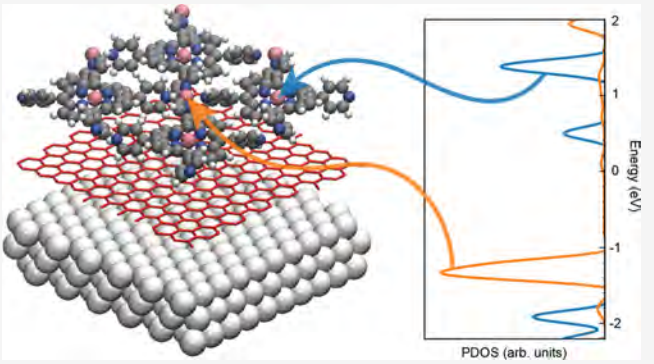

INTRODUCTION

Porphyrins constitute a rich class of organic molecules that, in nature, play a fundamental role in biological processes ranging from molecular transport to energy conversion.[1−3] These compounds are widely studied due to their broad range of potential applications such as in catalysis, organic solar cells, spectroscopic markers, sensors, and switches.[4−8] Indeed, porphyrins are very versatile, and their functionality can be tuned in different ways. The tetrapyrrolic macrocycle can host a variety of single-metal atoms,[9] which can behave as chemically active sites. Beside the inner atoms, the tuning of the porphyrin properties can also be achieved by exploiting the ability to bind different peripheral mesosubstituents. Molecules with particular substituents were shown to be ideal building blocks for the self-assembly of highly ordered two-dimensional architectures at surfaces.[1,10−12] The resulting patterns observed to form on many metallic substrates arise from the balance between the interaction of each molecule with the substrate and its neighboring molecules.[12] Therefore, the specificity of the substrate and, in some cases, even of the adsorption sites, combined with the molecular end-groups, determines the structure of the self-assembled pattern. Specifically, we consider 5,10,15,20-tetra(4-pyridyl)porphyrin (TPyP) with a single Co atom caged in the porphyrinic macrocycle (CoTPyP) and functionalized by four pyridinic end-groups, which can bind to an additional metal atom.[13] In this way, the outer groups become crucial for both the geometry of the molecular layer and the tuning of porphyrin's electronic properties. For instance, CoTPyP on Au(111) spontaneously forms an almost square lattice upon deposition of additional metal atoms that occupy the interstitial (pyridinic) sites among four adjacent molecules, offering a local atomic environment similar to the center of the macrocycle (iminic site)[10,14] (Figure 1a of ref 10). Those sites make the surface active toward different catalytic processes since they act as single atom catalysts.[10,15] The additional metal atoms could be both of the same species as the iminic one, forming a homo-metallic layer, or of different species, forming a hetero-metallic system. Furthermore, there is evidence that those peripheral atoms can further increase the catalytic activity of the layer well beyond the expected linear coverage-dependent behavior, suggesting a more complex mechanism between the two metal species.[10]

Received: August 17, 2023
Revised: November 6, 2023
Accepted: December 6, 2023
Published: January 19, 2024

The substrate can also play a role in the electronic structure and consequently on the chemical activity of the metal sites due to charge transfer with the molecular layer.[16−18]

In this work, the substrate is graphene (GR) on Ir(111). Indeed, GR on Ir(111) is almost freestanding, with a moiré characterized by a long periodicity and a small corrugation.[19,20] The small p-doping of GR with a shift of the Dirac cone of 0.07 eV away from the Fermi energy suggests only a small electron transfer from GR to the metallic substrate.[21,22] Since GR, in turn, is expected to interact only weakly with the molecular layer, the latter can therefore be well decoupled from the metal support, allowing us to focus on its intrinsic peculiarities.

In the following, we will discuss the striking lattice change from an ordered close-packed layer of CoTPyP/GR/Ir(111) (that we indicate as monometallic since Co atoms occupy only the macrocycle iminic sites) to a different close-packed structure induced by the deposition of further Co up to one additional metal atom per CoTPyP; we refer to this system, CoTPyP-Co/Gr/Ir(111), as bimetallic because of the occupation of the two different inequivalent sites (iminic and pyridinic) by metal atoms. These Co atoms were experimentally loaded via physical vapor deposition in UHV to form the CoTPyP-Co two-dimensional (2D) molecular layer (up to 9 wt %). The GR's weak interactions allow the Co atoms to be highly mobile from one side and increase the effective loading capabilities, and from the other side, they allow the porphyrins to freely rearrange in order to accommodate the additional metal.

We will report about geometry and electronic structure from a joint investigation including experimental surface science techniques [scanning tunneling microscopy (STM) and scanning tunneling spectroscopy (STS) performed in UHV] and ab initio density functional theory (DFT) simulations. We will show that the structural modification of the molecular layer is connected to deep peculiar changes of its properties and, in particular, to the different electronic and chemical identities of the two metal atoms. The results on the adsorption on GR of an individual molecule, functional for the entire study of mono- and bimetallic CoTPyP(-Co) layers, are first reported. Structures obtained as a function of Co loading are also discussed.

METHODS

Computational Details. The calculations were carried out using the Quantum ESPRESSO code[23−25] based on DFT, pseudopotentials, and plane waves. Slab geometries with periodic boundary conditions were employed. We used simulation cells with a height of 15 Å if the Ir slab is neglected (or 33 Å otherwise) and three different in-plane periodicities according to the specific system studied. The individual CoTPyP molecule was modeled both with and without Ir; in the first case, the unit cell has an in-plane hexagonal periodicity with lattice parameter a = 24.75 Å, corresponding to the GR/Ir(111) moiré pattern composed by (9 × 9) and (10 × 10) unit cells of Ir(111) and GR, respectively; in the second case, the unit cell has an in-plane rectangular periodicity with lattice parameters a = 17.22 Å, b = 17.04 Å containing a GR domain with 120C atoms. Both mono- and bimetallic layers, which form an oblique lattice, were simulated with cells with in-plane lattice parameters and angles, respectively, of a = 30.97 Å, b = 14.84 Å, and α = 63.8° (Figure S1) and a' = 28.36 Å, b' = 20.23 Å, and α' = 44.9° (Figure S2), containing two molecules each and 78 and 70 GR unit cells, respectively. In the two structures, the two molecules are rotated relative to each other by 65° and 90°, respectively. In both cases, the GR domain is slightly stretched compared to its ideal structure (which has a lattice parameter of 2.46 Å) in order to match the molecular layer and avoid the use of larger simulation cells. For the monometallic system, the adapted GR lattice parameter turns out to be 2.47 Å, while for the bimetallic system, the stretch applied to GR is slightly asymmetric, corresponding to a unit cell with in-plane primitive lattice vectors of 2.48 and 2.53 Å and an angle γ = 61.3° instead of 60°.

Spin-polarized calculations were carried out using the Perdew−Burke−Ernzerhof exchange correlation functional within the generalized gradient approximation method.[26] Vanderbilt ultrasoft pseudopotentials[27] were employed except for Co atoms, for which Rappe−Rabe−Kaxiras−Joannopoulos ultrasoft pseudopotentials[28] were used. The Hubbard-U correction[29] was introduced to improve the description of the metal atoms' 3d states, with a parameter U = 3.5 eV for Co in order to reproduce the 5.5 eV energy gap between occupied and unoccupied $3d_{z^2}$ levels reported in the literature.[30] Van der Waals interactions were also included using the Grimme-D3 approach.[31] We employed plane-wave cutoffs of 60 and 240 Ry for the wave function and the charge density, respectively. The Methfessel-Paxton smearing scheme was used for the occupation of electronic states with a smearing parameter of 0.01 Ry.[32] Geometrical optimizations were carried out using the Broyden−Fletcher−Goldfarb−Shanno algorithm with energy and force convergence thresholds of 1×10^{-6} Ry for the whole cell and 1×10^{-3} a.u. for each atomic force component, respectively. For the reciprocal space sampling, uniform grids of 4 × 4 × 1 and 8 × 8 × 1 k-points were employed, respectively, for self-consistent field (SCF) and nonself-consistent field (NSCF) calculations for the isolated CoTPyP molecule. For both mono- and bimetallic layers, instead, grids of 2 × 4 × 1 and 4 × 8 × 1 k-points were used for SCF and NSCF calculations. Electron density rearrangement plots due to the adsorption of an individual molecule or a molecular layer (M) on GR were calculated as the difference in the electron density distribution between the total system (M/GR) and the individual separated components in the positions assumed in the total system

$$\Delta n(\mathbf{r}) = n_{\mathrm{M/GR}}(\mathbf{r}) - (n_{\mathrm{M}}(\mathbf{r}) + n_{\mathrm{GR}}(\mathbf{r})) \quad (1)$$

The adsorption energy per molecule E_{ads} is defined as the difference between the total energy of the entire system $E_{\mathrm{M/GR}}$ and the sum of the two constituents (E_{M}, E_{GR}) divided by the number of molecules N_{M}

$$E_{\mathrm{ads}} = (E_{\mathrm{M/GR}} - (E_{\mathrm{M}} + E_{\mathrm{GR}}))/N_{\mathrm{M}} \quad (2)$$

The lateral intermolecular interaction energy per molecule E_{int} is defined as the difference between the total energy of the molecular layer E_{M} (without the substrate) divided by the number of molecules N_{M} and the energy of the individual molecule E_{m}

$$E_{\mathrm{int}} = E_{\mathrm{M}}/N_{\mathrm{M}} - E_{\mathrm{m}} \quad (3)$$

Hence, the more negative these values are, the stronger the adsorption and intermolecular interactions.

The STM and STS simulations were performed in a Tersoff-Hamann approach,[33] assuming a constant density of states for

https://doi.org/10.1021/acs.jpcc.3c05562
J. Phys. Chem. C 2024, 128, 1737−1745

the tip. For STM images, the integration range for the electronic density corresponds to the applied bias.

Experimental Details and Sample Preparation. STM experiments were carried out using a commercial Omicron low-temperature STM hosted at CNR-IOM Materials Foundry, Trieste, Italy, operated at 77 K under UHV conditions (base pressure estimated <7 × 10^{-11} mbar) and coupled with a preparation chamber equipped with a sputter gun, a sample annealing stage, LEED, and homemade organic and cobalt evaporators. STM topographic images were acquired in a constant-current mode and postprocessed with Gwyddion software with plane subtraction, line alignment, and drift correction. STS spectra were acquired with a lock-in amplifier set at a frequency of 1090 Hz and a bias modulation of 20 mV. The experimental error for the unit cell parameters is estimated to be <3%. The sample was prepared in the aforementioned preparation chamber with a base pressure of 1 × 10^{-10} mbar. The Ir(111) single crystal has been cleaned by standard cycles of Ar^+ sputtering (E = 2 keV) and annealing at 1200−1250 K and alternated with treatments in a 1 × 10^{-6} mbar oxygen background in the 570−1100 K temperature range. Before growing GR, the sample was finally annealed to 1250 K in UHV. GR was grown by thermal cracking of ethylene dosed from the background in vacuo. In detail, after the last annealing cycle, the sample has been cooled down to 1150 K and exposed for 5 min to 1 × 10^{-7} mbar of C_2H_4. The GR quality was checked by looking at the well-known LEED pattern, where no rotational domains could be observed, and higher-order diffraction spots of the GR moiré were visible. STM imaging of the bare GR reveals hundreds of nanometer-wide GR domains, with a defect density of the order of 0.01 nm^{-2} (Figure S3). The CoTPyP/GR/Ir(111) layers were grown *in vacuo* by the physical vapor deposition of the molecules on the GR substrate. Cobalt tetra-pyridyl-porphyrin chlorides [CoTPyPCl = 5,10,15,20-tetra(4-pyridyl)21*H*,23*H*-porphyrin Co(III) chloride] were purchased from Frontier Scientific. The molecular source was a heated boron nitride crucible. In order to remove the residual organic contaminants, the molecules have been kept at 500 K overnight for proper outgassing. The deposition time was 10 min, corresponding to about 0.3 ML estimated by direct STM inspection. The CoTPyP deposition on GR/Ir(111) was done with the sample kept at 500 K in a residual background pressure of 6 × 10^{-10} mbar, with a crucible temperature of about 600 K. The chloride ligand, which guarantees the chemical stability of the porphyrin in air, detaches from the molecule in the evaporation process.[10,13,34]

The CoTPyP-Co layer was formed by means of thermal sublimation from a resistively heated pure cobalt filament on the molecular layer already prepared, which was kept at 400 K to allow for the layer rearrangement and to avoid Co intercalation under GR and the formation of Co clusters.[35] At this temperature, the Co atoms are highly mobile on GR, and the ones that cannot be embedded in the molecular layer are found to form small (<1.0 nm apparent width) clusters on the bare GR moiré valleys (Figure S4). For the two layers that will be discussed later, the Co deposition was carried out at a constant rate of 0.06 ML/min (1 ML is referred to as a CoTPyP cell) for 3 and 18 min.

RESULTS AND DISCUSSION

Single CoTPyP Molecules. In order to focus on the molecule−support interaction, we first investigate with numerical simulations the adsorption of an individual CoTPyP molecule. We compare the adsorption on a free-standing GR layer and on GR/Ir(111) to elucidate the role of the iridium support.

As shown in Figure 1, the CoTPyP molecule on a free-standing GR layer assumes a C_{2v} symmetry due to the particular saddle shape of the molecular macrocycle. This was previously found on other supports [e.g., on Cu(111)[36] or Ag(111)[37]] and similarly for porphyrins with different peripheral end-groups.[38]

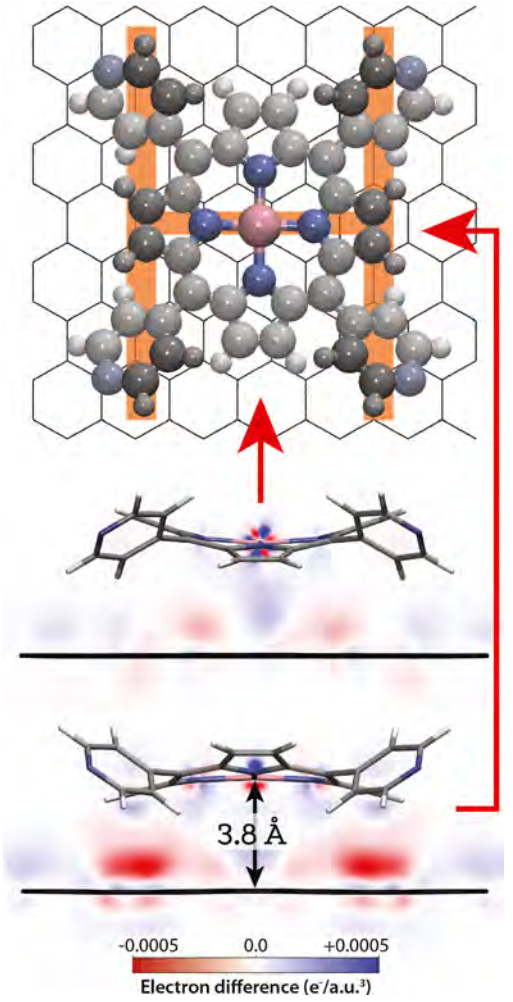

Figure 1. Individual CoTPyP molecules adsorbed on free-standing GR: optimized DFT model (ball-and-stick rendering for the top view and sticks only for the two side views), taken in the directions indicated by the arrows, with the calculated electron density rearrangement due to the interaction of the molecule with GR plotted on the reflection symmetry planes of the molecule passing through the Co atom and perpendicular to GR. The orange "H" sketched in the background in the top view highlights the C_{2v} symmetry of the molecule and passes through the pyrrolic rings tilted upward with respect to GR. Cobalt: pink; nitrogen: blue; hydrogen: light gray; and carbon: medium and dark (for atoms furthest from GR) gray.

The comparison with the free-standing CoTPyP molecule (Figure S5) clarifies the role of GR in the adsorption geometry. Indeed, the latter is a compromise resulting from the interaction with GR, which forces the pyridinic groups and the macrocycle to be as flat as possible, and from the steric

https://doi.org/10.1021/acs.jpcc.3c05562
J. Phys. Chem. C 2024, 128, 1737−1745

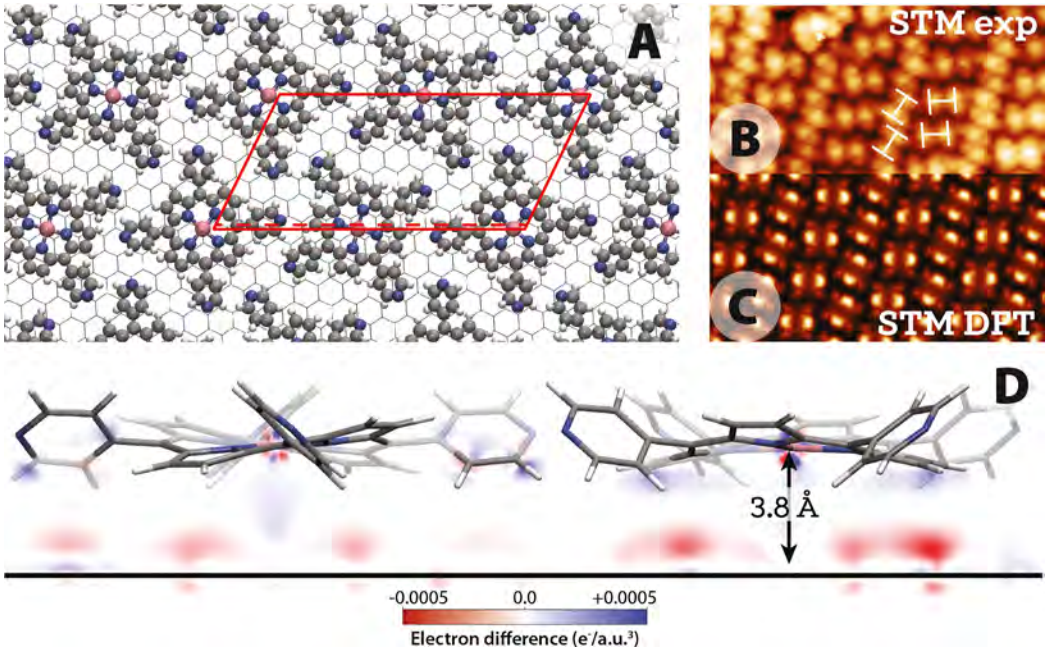

Figure 2. Monometallic CoTPyP molecular layer: (A) optimized DFT model (ball-and-stick rendering for the top view, with the supercell used; sticks only for the side view); (B) experimental STM image acquired at I = 100 pA and U_{bias} = −2.0 V. "H" shapes highlight the orientation of the molecules; (C) DFT-simulated STM image computed at a constant height of 2.25 Å above Co atoms; and (D) plot of the calculated electron density rearrangement due to the interaction between the molecular layer and GR on a plane perpendicular to GR and passing through the Co atoms of two adjacent molecules, parallel to the long side of the supercell (dashed red line).

repulsion between iminic and pyridinic hydrogen atoms. This leads to a distorted porphyrinic ring with the two pairs of opposite pyrroles inclined toward/away from the surface by $\psi \simeq \pm 18°$, while the pyridinic groups instead appear to be rotated alternatively clock- and anticlockwise by $\theta \simeq 38°$ with respect to GR. This saddle shape is more or less pronounced according to the strength of the substrate−adsorbate interaction. For MnTPyPs on the more strongly interacting Cu(111) substrate, pyridinic groups and the pyrroles pointing downward are predicted to be flatter, with $\theta = 29.8 \pm 1.8°$ and $\psi = -14.6 \pm 0.9°$, while pyrroles pointing upward are more inclined ($\psi = 24.7 \pm 1.5°$),[39] and an angle $\theta = 30 \pm 5°$ was predicted for 2HTPyPs on Ag(111).[37] In our case, the distance between the Co metal atom and the substrate is 3.8 Å, and the minimum distance between the hydrogen terminations and the substrate is 2.5−2.6 Å; the same distances characterize H−H steric interactions. Similar values are also observed for other molecules with cyclic groups.[40]

The calculated adsorption energy per molecule is E_{ads} = −1.95 eV and can be attributed mainly to van der Waals interactions. There are neither preferential adsorption sites nor preferential registries; upon rotations or translations parallel to the GR plane, neither the molecular structure nor the adsorption energy change, suggesting optimal conditions for diffusion and self-assembly.

Upon adsorption of the CoTPyP molecule, GR remains perfectly flat and there is no charge transfer; hence, its DOS remains unaffected with Dirac points located at Fermi energy. GR thus acts only as a weakly interacting support for the isolated molecule, determining its geometrical conformation and inducing a small charge rearrangement, as shown in Figure 1.

For comparison, we also considered the case of GR supported on a three-layer Ir(111) slab. GR on iridium is known to form a moiré structure characterized by a long periodicity [10 × 10 GR unit cells on 9 × 9 Ir(111) surface unit cells] with an average distance of 3.50 Å from Ir and a small corrugation of about 0.30 Å.[41] The GR moiré pattern is preserved upon adsorption of a single CoTPyP molecule (Figure S6); no pinning of GR toward Ir is observed, at variance with phthalocyanines on the same substrate,[42] but only a 0.02 Å decrease in the GR-Ir distance under the CoTPyP. On the other side, the structure of the adsorbed molecule does not change taking or not taking into account the Ir substrate. These findings justify neglecting the Ir substrate in our simulations.

Monometallic CoTPyP Layers. We now focus on a single layer of CoTPyP. STM topographic images acquired at negative bias (Figure 2 panel B) reveal the formation of a staggered arrangement made by rows of molecules with alternating orientation, where molecular centers form an almost hexagonal structure with angles of 60.0 ± 3.8° (see Figure S1 for details). This is not only similar to the supramolecular architecture formed by 2HTPyPs on Ag(111)[37] and FeTPyP on Au(111)[43] but also by tetraphenylporphyrins on Ag(111).[44] Starting from the experimental observations both in direct (STM images in Figure 2 panel B and Figure S7 panel A) and in reciprocal space [with the corresponding fast Fourier transform (FFT) in Figure S7 panel B], we describe this structure as an oblique lattice with cell parameters a = 31.0 Å, b = 14.8 Å, and α = 63.8° and two inequivalent CoTPyP molecules in the unit cell, rotated one relative to another by an azimuthal angle of 65°. The DFT results indicate that the interaction of a molecule with the substrate in a self-assembled layer is not different from that of an isolated molecule. The DOS of both CoTPyP and GR are unchanged, and no transfer but only a tiny redistribution of charge is observed, smaller than 0.005 au

https://doi.org/10.1021/acs.jpcc.3c05562
J. Phys. Chem. C 2024, 128, 1737−1745

(Figure 2 panel D). The computed adsorption energy for each molecule is $E_{ads} = -1.72$ eV, only slightly weaker than that of the single molecule case. The geometric conformation of an adsorbed molecule isolated or in a molecular layer is the same, confirming that the substrate is mainly responsible for the internal distortion. On the other side, hundreds of nanometer-wide islands are observed, suggesting a relevant lateral intermolecular interaction that was estimated to be equal to $E_{int} = -0.41$ eV/molecule. Also, in this case, neither a specific adsorption site nor a specific registry with GR is found, either from the experimental STM images or from the DFT calculations, suggesting that the self-assembly is exclusively driven by the lateral intermolecular interactions.

CoTPyP-Co Bimetallic Layers. The molecular layer offers peripheral sites among neighboring molecules that can be occupied by additional metal atoms, which directly bind to the pyridinic nitrogen terminations as we suggested in a previous paper on the basis of NEXAFS measurements.[13] Remarkably, the deposition of Co atoms causes a radical change in the molecular arrangement, which we address in detail in the following section. The loading of adatoms is quantified with respect to the number of CoTPyP molecules (i.e., $\theta_{Co}/\theta_{CoTPyP}$).

At low Co coverage ($\theta_{Co}/\theta_{CoTPyP} \lesssim 0.25$), the Co atoms landing on the surface bind together four CoTPyPs through their pyridinic terminations so as to reach tetra-coordination. Those four molecules rearrange their relative positions, forming a rigid, almost square $(CoTPyP)_4Co$ block (Figure 3 panel A). The STM image also reveals that the block has a precise chirality due to a specific orientation of the four CoTPyP molecules, which are rotated by 90° with respect to the neighboring ones, as highlighted by the "H"-like shapes. As a consequence, all the pyridinic rings pointing to Co have the same inclination with respect to the substrate and donate a specific chirality to the molecular assembly.

At a Co coverage $\theta_{Co}/\theta_{CoTPyP} = 0.25$, a regular arrangement of such blocks is visible, forming an almost square lattice with an apparent 2×2 periodicity (Figure 3 panel B). However, a closer inspection of this image, where the molecular orientation (the "H" shape) is visible, reveals that adjacent blocks have opposite chirality, which makes the actual periodicity larger, i.e., $(2\sqrt{2} \times 2\sqrt{2})R45°$ (the red cell in panel D). Chiral features are also visible in the STM image in panel C, taken at a different bias. Here, green "pinwheels" centered on one molecular block every two in a chessboard pattern are sketched to guide the eye.

We built an atomistic model assembling the *H*-shaped molecules in a molecular architecture compatible with the experimental STM images for periodicity and chirality; the top view is shown in panel D, where the blue and red cells indicate, respectively, the apparent 2×2 and the actual $(2\sqrt{2} \times 2\sqrt{2})R45°$ periodicities. Since performing a full DFT calculation of such a large structure is computationally very demanding, we simulate its electron density distribution by considering the superposition of Gaussians centered at the atomic sites (Figure 3 panel E); the corresponding map is in good agreement with the experimental image in panel C and shows that the "arms" of the pinwheels originate from the pyridinic rings not involved in the bonding with the peripheral Co centers.

When the relative coverage of the deposited Co atoms is increased, a further reordering takes place. Once again, we

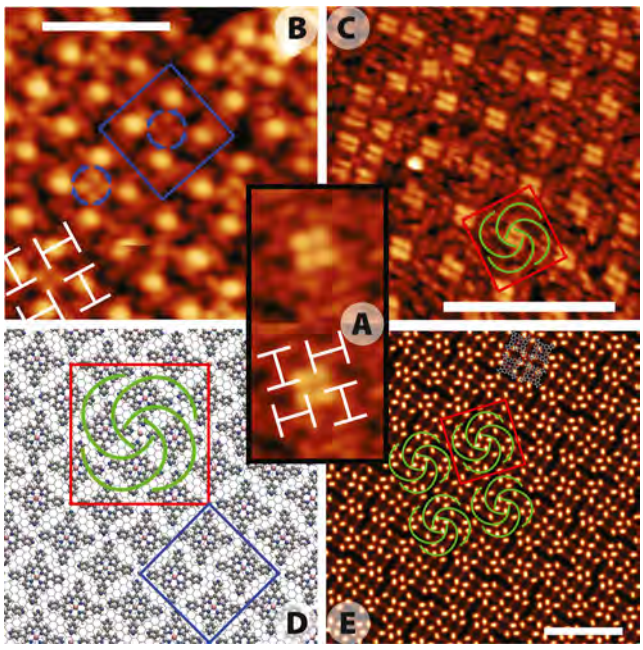

Figure 3. Experimental STM images and models for an unsaturated molecular layer: (A) STM image of a single $(CoTPyP)_4Co$ block acquired at $I = 60$ pA and $U_{bias} = +2.0$ V; the superimposed "H" shapes highlight the orientation of the molecules, and the blue cell indicates the apparent 2×2 periodicity; (B) STM image of a domain with a regular periodicity and a peripheral Co coverage $\theta_{Co}/\theta_{CoTPyP} = 0.25$ acquired at $I = 100$ pA and $U_{bias} = +2.0$ V; circular arrows indicate the different chirality of two adjacent $(CoTPyP)_4Co$ blocks, and the red cell indicates the effective $(2\sqrt{2} \times 2\sqrt{2})R45°$ periodicity (scale bar 4 nm); (C) STM image of a different domain with the same periodicity and Co coverage of (B) acquired at $I = 100$ pA and $U_{bias} = +1.4$ V; the superimposed "pinwheel" highlights the chiral structure (scale bar 10 nm); (D) model of the periodic layer of (B,C), with the blue cell representing the apparent 2×2 periodicity and the red supercell representing the true $(2\sqrt{2} \times 2\sqrt{2})R45°$ periodicity that takes into account the chiral structure; (E) topographic map at 3.0 Å above Co atoms for the model in (D) obtained by considering a superposition of 3D Gaussians with $\sigma = 0.5$ Å centered on the atomic sites of the model (scale bar 5 nm). A version of the image without superimposed drawings is reported in Figure S8.

notice that the Co location is not random since it preferentially binds laterally to the $(CoTPyP)_4Co$ blocks rather than diagonally. Small chains and domains with a local 1×1 ($\theta_{Co}/\theta_{CoTPyP} = 1$) periodicity start forming, suggesting a different rearrangement of the neighboring molecules. In Figure 4 (panel A), it is possible to distinguish the orientation of the molecules in such compact domains (with "H" shapes indicated to guide the eye), once again yielding structures with alternate chirality.

At full peripheral metal loading (i.e., $\theta_{Co}/\theta_{CoTPyP} = 1$) over wide domains (Figure 4 panel B), the deposited atoms and the molecular centers form an almost perfect square lattice with an apparent 1×1 periodicity (the centers of nearest neighboring molecules are distant 14.23 ± 0.05 Å and the jointing vectors form angles of $90 \pm 0.5°$). On a larger scale (Figure S9), it can be observed that saturation is achieved first at the border of the CoTPyP islands, probably due to the major exposure to the mobile Co atoms coming to diffuse on the bare GR and thanks to the greater degree of movement that peripheral molecules have with respect to the ones in the 2D bulk. For this reason, it is common to find tens of nanometer-wide fully saturated

https://doi.org/10.1021/acs.jpcc.3c05562
J. Phys. Chem. C 2024, 128, 1737−1745

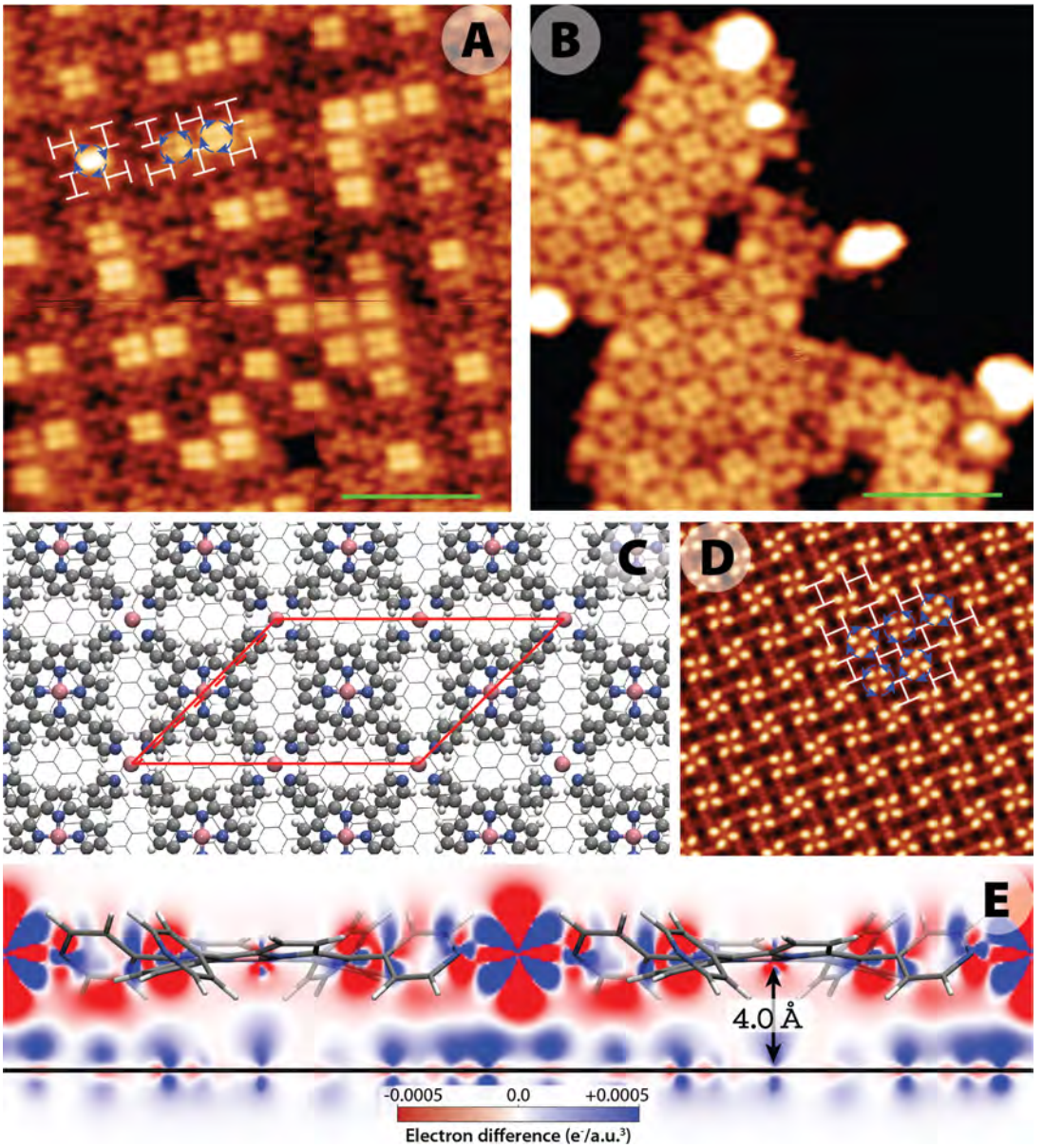

Figure 4. Bimetallic CoTPyP-Co molecular layer: (A) experimental STM image at partial peripheral Co coverage, acquired at I = 60 pA and U_{bias} = +2.5 V with superimposed H-model shapes highlighting the molecular orientation (scale bar 5 nm); (B) experimental STM image at full peripheral Co coverage ($\theta_{Co}/\theta_{CoTPyP}$ = 1) acquired at I = 50 pA and U_{bias} = +2.2 V(scale bar 5 nm); (C) optimized DFT model (ball-and-stick rendering for the top view, with the supercell used; sticks only for the side view); (D) plot of the calculated electron density rearrangement due to the interaction between the molecular layer and GR on a plane perpendicular to GR and passing through the additional Co atoms, parallel to the short side of the supercell; (E) simulated STM image computed at a constant height of 2.25 Å above Co atoms.

islands that have completely detached from the rest of the layer, such as the one presented in Figure 4 panel B. Closer inspection indicates a precise chiral structure also in the saturated layer. The local chirality around the pyridinic Co atoms inverts at every adjacent site, and therefore, the global arrangement has a chessboard structure, which can be described by an oblique lattice (panel C). The atomistic model in this case is affordable by full DFT calculations and has been optimized, giving a unit cell with primitive vectors a = 28.4 Å, b = 20.2 Å, and angle α = 44.9° and with two inequivalent molecules rotated by 90° relative to each other (see Figure 4 panel C and Figure S2 for more details). These lattice parameters were optimized starting from the experimental data (Figure S10). As mentioned, no relevant modifications of the individual molecular shape are found with respect to the monometallic case, apart from a small increase in the CoTPyP-GR distance from ≃3.8 to ≃4.0 Å, accompanied by an increase of the pyridinic rotation angle to θ = 38.3 ± 0.8°.

Interestingly, the actual ordering of the evaporated Co atoms, at all loadings, is evidently not random, suggesting a long-range (>3 nm) repulsive interaction between peripheral metal atoms. The nature of such an interaction is currently not clear, but we think it could stem from the geometrical hindrance caused by the molecules rearrangement or, more interestingly, from a pyridyl-mediated antiferromagnetic coupling, as previously predicted by DFT regarding the free-standing CoTPyPCo layer.[45] Hence, it is worth saying that in

https://doi.org/10.1021/acs.jpcc.3c05562
J. Phys. Chem. C 2024, 128, 1737−1745

our calculation where GR is present, we do not observe such a magnetic coupling.

Despite the 5% higher molecular-substrate distance, at full peripheral Co loading, a stronger interaction with the substrate is predicted with respect to the monometallic case, as proved by a bit higher adsorption energy of 2.07 eV per molecular layer unit (composed of one CoTPyP and one peripheral Co) that has to be related to a net charge transfer from the molecular layer to GR. Indeed, the GR Dirac cone is located at −0.5 eV with respect to the Fermi energy (Figure 5 panel A).

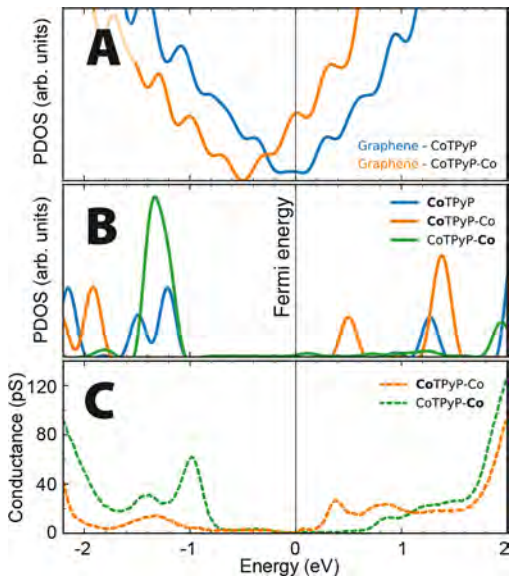

Figure 5. Computed projected density of states (PDOS) (solid lines) and experimental STS measurements (dashed lines). (A) PDOS on C atoms of GR for both mono- and bimetallic layers; (B) PDOS on both Co species in mono- and bimetallic layers; and (C) experimental STS measurements acquired on iminic and pyridinic Co atoms in the bimetallic layer (starting set point was 2 V and 0.2 A).

Considering a linear DOS of GR around the Fermi energy, which is a good approximation in the ±1 eV range, i.e., $D(E) = D_0|E|$, with D_0 = 0.09 eV^2 per GR unit cell,[46] we find by integration that the number of transferred electrons is $N = \pm D_0\Delta E_F^2/2$ leading to 0.42 e$^-$ transferred from each molecular layer unit to GR. This is evident also in the charge density difference plot (Figure 4 panel E), where a significant charge redistribution takes place between GR and the molecular layer, with major contributions coming from the peripheral metallic atoms and the pyridinic groups.

Even if the two Co species are both tetra-coordinated with nitrogen atoms, DFT calculations predict different identities. Indeed, the iminic one is characterized by a + 2 oxidation state and $a \sim 1\ \mu_B$ magnetic moment, whereas the pyridinic one is characterized by a + 1 oxidation state and doubled magnetization. This is related to the different occupation of the atomic orbitals in the two inequivalent atoms, although their charge is the same. This different electronic structure is also reflected in experimental STS maps for the bimetallic system (bottom panel in Figure 5). Here, the inequivalence between the two Co species can be clearly observed by looking at molecular states located in the −2 to +2 eV range. Interestingly, with respect to the chemical activity of the two nonequivalent sites, this difference in oxidation states paves the way toward specific selectivities or cooperative catalytic processes on the surface.[47]

Focusing on the iminic metal atoms, no variations in orbital occupation and consequently in total magnetization and oxidation state between mono- and bimetallic systems show up from ab initio calculations. This suggests that the layer reorganization and the additional peripheral metallic centers do not substantially affect the porphyrinic core. The only relevant change is related to the DOS where, even if all features related to iminic Co remain identical, a rigid shift of 0.6−0.7 eV occurs toward negative energies in the bimetallic case. This has to be also related to the drastic change in the work function, which is predicted to vary from 4.3 eV for the monometallic case to 3.1 eV for the bimetallic one. The work function is particularly relevant for the catalytic aspect since it is known that the presence of a surface dipole can have a (de)stabilizing effect toward surface species, simply explained in terms of electrostatic interactions and more importantly toward polar solvents within an electrocatalytic scenario.[48]

CONCLUSIONS

In summary, we have investigated the modification of a self-assembled CoTPyP layer on an Ir(111)-supported GR sheet induced by the addition of single cobalt atoms that occupy intermolecular sites binding to four adjacent molecules. The intra- and intermolecular metal centers, although both tetracoordinated to the nitrogen atoms, have a different orbital occupancy and oxidation state (+2 in the macrocycle and + 1 at the intermolecular site), thus offering the potential for different and tunable catalytic properties. The addition of peripheral metal atoms causes a radical rearrangement of the molecular network that depends on the local adatom coverage, yielding geometries that vary from nearly hexagonal to nearly square in the case of full coverage (i.e., one additional Co for each CoTPyP). The saddle shape of the molecules combined with their relative orientation originates peculiar chiral features in the bimetallic network, at both full and intermediate coverage. Another drastic effect of the addition of the peripheral atoms is a reduction of about 1 eV of the work function of the system, from 4.3 eV for the monometallic case to 3.1 eV for the bimetallic one with full coverage of the peripheral atoms.

ASSOCIATED CONTENT

Supporting Information

The Supporting Information is available free of charge at https://pubs.acs.org/doi/10.1021/acs.jpcc.3c05562.

Monometallic CoTPyP simulation cell; bimetallic CoTPyP-Co simulation cell; STM image on bare GR; STM image of CoTPyP-Co/GR/Ir(111) at $\theta_{Co}/\theta_{CoTPyP} \simeq 0.25$; optimized model for a single CoTPyP molecule in vacuum; optimized configuration of a single CoTPyP on GR/Ir(111); STM image of CoTPyP/Gr/Ir(111) and corresponding FFT; experimental STM image and models for an unsaturated molecular layer; long range STM image of CoTPyP-Co/GR/Ir(111); STM image of CoTPyP-Co/GR/Ir(111) and corresponding FFT; DFT electrostatic potential profile of both monometallic CoTPyP and bimetallic (CoTPyP)Co molecular layers; STM images for the monometallic layer at different biases; and STM image of the bimetallic layer at different biases (PDF)

DFT-optimized atomic positions and 3D rendering of the structures (ZIP)

https://doi.org/10.1021/acs.jpcc.3c05562
J. Phys. Chem. C 2024, 128, 1737−1745

AUTHOR INFORMATION

Corresponding Author

Maria Peressi − *Department of Physics, University of Trieste, 34127 Trieste, Italy; ICSC - Italian Research Center on High Performance Computing, Big Data and Quantum Computing, Casalecchio di Reno, Bologna 40033, Italy;* orcid.org/0000-0001-6142-776X; Email: peressi@units.it

Authors

Davide Bidoggia − *Department of Physics, University of Trieste, 34127 Trieste, Italy;* orcid.org/0000-0002-0757-1397

Francesco Armillotta − *Department of Physics, University of Trieste, 34127 Trieste, Italy; Institut de Physique des Nanostructures, Ecole Polytechnique Fédérale de Lausanne (EPFL), CH-1015 Lausanne, Switzerland;* orcid.org/0000-0001-7247-6428

Alessandro Sala − *CNR-IOM, Area Science Park, 34149 Trieste, Italy;* orcid.org/0000-0002-5845-1301

Erik Vesselli − *Department of Physics, University of Trieste, 34127 Trieste, Italy; CNR-IOM, Area Science Park, 34149 Trieste, Italy; Center for Energy, Environment and Transport Giacomo Ciamician, University of Trieste, 34127 Trieste, Italy;* orcid.org/0000-0002-6799-0032

Complete contact information is available at: https://pubs.acs.org/10.1021/acs.jpcc.3c05562

Notes

The authors declare no competing financial interest.

ACKNOWLEDGMENTS

The authors acknowledge financial support from MUR (PRIN Bando 2017 grant no. 2017KFY7XF). E.V. acknowledges support from MUR under the project PRIN 2022XXJNRS. M.P. acknowledges support from the Fondazione ICSC—"Italian Research Center on High-Performance Computing, Big Data, and Quantum Computing"—Spoke 7, Materials and Molecular Sciences—National Recovery and Resilience Plan (PNRR)—funded by MUR Missione 4—Componente 2—Investimento 1.4—Next Generation EU (NGEU). Computational resources have been obtained from CINECA through the ISCRA initiative and the agreement with the University of Trieste.

REFERENCES

(1) Vesselli, E. Tetrapyrroles at near-ambient pressure: porphyrins and phthalocyanines beyond the pressure gap. *J. Phys. Mater.* **2020**, *3*, 022002.

(2) Meunier, B. Metalloporphyrins as versatile catalysts for oxidation reactions and oxidative DNA cleavage. *Chem. Rev.* **1992**, *92*, 1411−1456.

(3) Huang, X.; Groves, J. T. Oxygen Activation and Radical Transformations in Heme Proteins and Metalloporphyrins. *Chem. Rev.* **2018**, *118*, 2491−2553.

(4) Haddad, R. E.; Gazeau, S.; Pécaut, J.; Marchon, J.-C.; Medforth, C. J.; Shelnutt, J. A. Origin of the Red Shifts in the Optical Absorption Bands of Nonplanar Tetraalkylporphyrins. *J. Am. Chem. Soc.* **2003**, *125*, 1253−1268.

(5) Hulsken, B.; Van Hameren, R.; Gerritsen, J. W.; Khoury, T.; Thordarson, P.; Crossley, M. J.; Rowan, A. E.; Nolte, R. J. M.; Elemans, J. A. A. W.; Speller, S. Real-time single-molecule imaging of oxidation catalysis at a liquid−solid interface. *Nat. Nanotechnol.* **2007**, *2*, 285−289.

(6) Moresco, F.; Meyer, G.; Rieder, K.-H.; Tang, H.; Gourdon, A.; Joachim, C. Conformational Changes of Single Molecules Induced by Scanning Tunneling Microscopy Manipulation: A Route to Molecular Switching. *Phys. Rev. Lett.* **2001**, *86*, 672−675.

(7) Flechtner, K.; Kretschmann, A.; Steinrück, H. P.; Gottfried, J. M. NO-Induced Reversible Switching of the Electronic Interaction between a Porphyrin-Coordinated Cobalt Ion and a Silver Surface. *J. Am. Chem. Soc.* **2007**, *129*, 12110−12111.

(8) Campbell, W. M.; Burrell, A. K.; Officer, D. L.; Jolley, K. W. Porphyrins as light harvesters in the dye-sensitised TiO2 solar cell. *Coord. Chem. Rev.* **2004**, *248*, 1363−1379.

(9) Gottfried, J. M. Surface chemistry of porphyrins and phthalocyanines. *Surf. Sci. Rep.* **2015**, *70*, 259−379.

(10) Wurster, B.; Grumelli, D.; Hötger, D.; Gutzler, R.; Kern, K. Driving the Oxygen Evolution Reaction by Nonlinear Cooperativity in Bimetallic Coordination Catalysts. *J. Am. Chem. Soc.* **2016**, *138*, 3623−3626.

(11) Auwärter, W.; Seufert, K.; Klappenberger, F.; Reichert, J.; Weber-Bargioni, A.; Verdini, A.; Cvetko, D.; Dell'Angela, M.; Floreano, L.; Cossaro, A.; et al. Site-specific electronic and geometric interface structure of Co-tetraphenyl-porphyrin layers on Ag(111). *Phys. Rev. B: Condens. Matter Mater. Phys.* **2010**, *81*, 245403.

(12) Kumar, A.; Banerjee, K.; Liljeroth, P. Molecular assembly on two-dimensional materials. *Nanotechnology* **2017**, *28*, 082001.

(13) Armillotta, F.; Bidoggia, D.; Biasin, P.; Annese, A.; Cossaro, A.; Verdini, A.; Floreano, L.; Peressi, M.; Vesselli, E. Spectroscopic fingerprints of iron-coordinated cobalt and iron porphyrin layers on graphene. *Cell Rep. Phys. Sci.* **2023**, *4*, 101378.

(14) Liu, B.; Zhang, S.; Miao, G.; Guo, J.; Meng, S.; Wang, W. Inspecting the nonbonding and antibonding orbitals in a surface-supported metal−organic framework. *Chem. Commun.* **2021**, *57*, 4580−4583.

(15) Armillotta, F.; Bidoggia, D.; Baronio, S.; Biasin, P.; Annese, A.; Scardamaglia, M.; Zhu, S.; Bozzini, B.; Modesti, S.; Peressi, M.; et al. Single Metal Atom Catalysts and ORR: H-Bonding, Solvation, and the Elusive Hydroperoxyl Intermediate. *ACS Catal.* **2022**, *12*, 7950−7959.

(16) Lukasczyk, T.; Flechtner, K.; Merte, L. R.; Jux, N.; Maier, F.; Gottfried, J. M.; Steinrück, H. P. Interaction of Cobalt(II) Tetraarylporphyrins with a Ag(111) Surface Studied with Photoelectron Spectroscopy. *J. Phys. Chem. C* **2007**, *111*, 3090−3098.

(17) Diller, K.; Klappenberger, F.; Allegretti, F.; Papageorgiou, A. C.; Fischer, S.; Wiengarten, A.; Joshi, S.; Seufert, K.; Écija, D.; Auwärter, W.; et al. Investigating the molecule-substrate interaction of prototypic tetrapyrrole compounds: Adsorption and self-metalation of porphine on Cu(111). *J. Chem. Phys.* **2013**, *138*, 154710.

(18) Hieringer, W.; Flechtner, K.; Kretschmann, A.; Seufert, K.; Auwärter, W.; Barth, J. V.; Görling, A.; Steinrück, H. P.; Gottfried, J. M. The Surface Trans Effect: Influence of Axial Ligands on the Surface Chemical Bonds of Adsorbed Metalloporphyrins. *J. Am. Chem. Soc.* **2011**, *133*, 6206−6222.

(19) Meng, L.; Wu, R.; Zhang, L.; Li, L.; Du, S.; Wang, Y.; Gao, H.-J. Multi-oriented moiré superstructures of graphene on Ir(111): experimental observations and theoretical models. *J. Phys.: Condens. Matter* **2012**, *24*, 314214.

(20) Hämäläinen, S. K.; Boneschanscher, M. P.; Jacobse, P. H.; Swart, I.; Pussi, K.; Moritz, W.; Lahtinen, J.; Liljeroth, P.; Sainio, J. Structure and local variations of the graphene moiré on Ir(111). *Phys. Rev. B: Condens. Matter Mater. Phys.* **2013**, *88*, 201406.

(21) Larciprete, R.; Ulstrup, S.; Lacovig, P.; Dalmiglio, M.; Bianchi, M.; Mazzola, F.; Hornekær, L.; Orlando, F.; Baraldi, A.; Hofmann, P.; et al. Oxygen Switching of the Epitaxial Graphene−Metal Interaction. *ACS Nano* **2012**, *6*, 9551−9558.

(22) Ulstrup, S.; Schüler, M.; Bianchi, M.; Fromm, F.; Raidel, C.; Seyller, T.; Wehling, T.; Hofmann, P. Manifestation of nonlocal electron-electron interaction in graphene. *Phys. Rev. B* **2016**, *94*, 081403.

(23) Giannozzi, P.; Baroni, S.; Bonini, N.; Calandra, M.; Car, R.; Cavazzoni, C.; Ceresoli, D.; Chiarotti, G. L.; Cococcioni, M.; Dabo,

I.; et al. QUANTUM ESPRESSO: a modular and open-source software project for quantum simulations of materials. *J. Phys.: Condens. Matter* **2009**, *21*, 395502.
(24) Giannozzi, P.; Andreussi, O.; Brumme, T.; Bunau, O.; Nardelli, M. B.; Calandra, M.; Car, R.; Cavazzoni, C.; Ceresoli, D.; Cococcioni, M.; et al. Advanced capabilities for materials modelling with Quantum ESPRESSO. *J. Phys.: Condens. Matter* **2017**, *29*, 465901.
(25) Giannozzi, P.; Baseggio, O.; Bonfà, P.; Brunato, D.; Car, R.; Carnimeo, I.; Cavazzoni, C.; de Gironcoli, S.; Delugas, P.; Ruffino, F. F.; et al. QuantumESPRESSO toward the exascale. *J. Chem. Phys.* **2020**, *152*, 154105.
(26) Perdew, J. P.; Burke, K.; Ernzerhof, M. Generalized Gradient Approximation Made Simple. *Phys. Rev. Lett.* **1996**, *77*, 3865−3868.
(27) Vanderbilt, D. Soft self-consistent pseudopotentials in a generalized eigenvalue formalism. *Phys. Rev. B: Condens. Matter Mater. Phys.* **1990**, *41*, 7892−7895.
(28) Rappe, A. M.; Rabe, K. M.; Kaxiras, E.; Joannopoulos, J. D. Optimized pseudopotentials. *Phys. Rev. B: Condens. Matter Mater. Phys.* **1990**, *41*, 1227−1230.
(29) Cococcioni, M.; de Gironcoli, S. Linear response approach to the calculation of the effective interaction parameters in the LDA+U method. *Phys. Rev. B: Condens. Matter Mater. Phys.* **2005**, *71*, 035105.
(30) da Silva, L. G. G. V. D.; Tiago, M. L.; Ulloa, S. E.; Reboredo, F. A.; Dagotto, E. Many-body electronic structure and Kondo properties of cobalt-porphyrin molecules. *Phys. Rev. B: Condens. Matter Mater. Phys.* **2009**, *80*, 155443.
(31) Grimme, S.; Antony, J.; Ehrlich, S.; Krieg, H. A consistent and accurate ab initio parametrization of density functional dispersion correction (DFT-D) for the 94 elements H-Pu. *J. Chem. Phys.* **2010**, *132*, 154104.
(32) Methfessel, M.; Paxton, A. T. High-precision sampling for Brillouin-zone integration in metals. *Phys. Rev. B: Condens. Matter Mater. Phys.* **1989**, *40*, 3616−3621.
(33) Tersoff, J.; Hamann, D. R. Theory of the scanning tunneling microscope. *Phys. Rev. B: Condens. Matter Mater. Phys.* **1985**, *31*, 805−813.
(34) Murphy, B. E.; Krasnikov, S. A.; Sergeeva, N. N.; Cafolla, A. A.; Preobrajenski, A. B.; Chaika, A. N.; Lübben, O.; Shvets, I. V. Homolytic Cleavage of Molecular Oxygen by Manganese Porphyrins Supported on Ag(111). *ACS Nano* **2014**, *8*, 5190−5198.
(35) Decker, R.; Brede, J.; Atodiresei, N.; Caciuc, V.; Blügel, S.; Wiesendanger, R. Atomic-scale magnetism of cobalt-intercalated graphene. *Phys. Rev. B: Condens. Matter Mater. Phys.* **2013**, *87*, 041403.
(36) Zhang, Q.; Kuang, G.; Pang, R.; Shi, X.; Lin, N. Switching Molecular Kondo Effect via Supramolecular Interaction. *ACS Nano* **2015**, *9*, 12521−12528.
(37) Auwärter, W.; Weber-Bargioni, A.; Riemann, A.; Schiffrin, A.; Gröning, O.; Fasel, R.; Barth, J. V. Self-assembly and conformation of tetrapyridyl-porphyrin molecules on Ag(111). *J. Chem. Phys.* **2006**, *124*, 194708.
(38) Castellarin-Cudia, C.; Borghetti, P.; Di Santo, G.; Fanetti, M.; Larciprete, R.; Cepek, C.; Vilmercati, P.; Sangaletti, L.; Verdini, A.; Cossaro, A.; et al. Substrate Influence for the Zn-tetraphenyl-porphyrin Adsorption Geometry and the Interface-Induced Electron Transfer. *ChemPhysChem* **2010**, *11*, 2248−2255.
(39) Chen, X.; Lei, S.; Lotze, C.; Czekelius, C.; Paulus, B.; Franke, K. J. Conformational adaptation and manipulation of manganese tetra(4-pyridyl)porphyrin molecules on Cu(111). *J. Chem. Phys.* **2017**, *146*, 092316.
(40) Laplaza, R.; Boto, R. A.; Contreras-García, J.; Montero-Campillo, M. M. Steric clash in real space: biphenyl revisited. *Phys. Chem. Chem. Phys.* **2020**, *22*, 21251−21256.
(41) Podda, N.; Corva, M.; Mohamed, F.; Feng, Z.; Dri, C.; Dvorak, F.; Matolin, V.; Comelli, G.; Peressi, M.; Vesselli, E. Experimental and Theoretical Investigation of the Restructuring Process Induced by CO at Near Ambient Pressure: Pt Nanoclusters on Graphene/Ir(111). *ACS Nano* **2017**, *11*, 1041−1053.
(42) Altenburg, S. J.; Lattelais, M.; Wang, B.; Bocquet, M.-L.; Berndt, R. Reaction of Phthalocyanines with Graphene on Ir(111). *J. Am. Chem. Soc.* **2015**, *137*, 9452−9458.
(43) Stein, A.; Rolf, D.; Lotze, C.; Czekelius, C.; Franke, K. J.; Tegeder, P. Electronic structure of an iron porphyrin derivative on Au(1 1 1). *J. Phys.: Condens. Matter* **2019**, *31*, 044002.
(44) Buchner, F.; Kellner, I.; Hieringer, W.; Görling, A.; Steinrück, H. P.; Marbach, H. Ordering aspects and intramolecular conformation of tetraphenylporphyrins on Ag(111). *Phys. Chem. Chem. Phys.* **2010**, *12*, 13082.
(45) Mandal, B.; Chung, J. S.; Kang, S. G. Theoretical Insight into M1TPyP-M2 (M1, M2 = Fe, Co) MOFs: Correlation between Electronic Structure and Catalytic Activity Extending to Potentiality in Capturing Flue Gases. *J. Phys. Chem. C* **2018**, *122*, 9899−9908.
(46) Giovannetti, G.; Khomyakov, P. A.; Brocks, G.; Karpan, V. M.; van den Brink, J.; Kelly, P. J. Doping Graphene with Metal Contacts. *Phys. Rev. Lett.* **2008**, *101*, 026803.
(47) Jeong, H.; Shin, D.; Kim, B.-S.; Bae, J.; Shin, S.; Choe, C.; Han, J. W.; Lee, H. Controlling the Oxidation State of Pt Single Atoms for Maximizing Catalytic Activity. *Angew. Chem., Int. Ed.* **2020**, *59*, 20691−20696.
(48) Martinez, U.; Giordano, L.; Pacchioni, G. Tuning the work function of ultrathin oxide films on metals by adsorption of alkali atoms. *J. Chem. Phys.* **2008**, *128*, 164707.

https://doi.org/10.1021/acs.jpcc.3c05562
J. Phys. Chem. C 2024, 128, 1737−1745